frontiers | Frontiers in Marine Science

TYPE Original Research
PUBLISHED 04 November 2024
DOI 10.3389/fmars.2024.1304930

OPEN ACCESS

EDITED BY
Johan Schijf,
University of Maryland, United States

REVIEWED BY
Chen-Feng You,
National Cheng Kung University, Taiwan
Toshihiro Yoshimura,
Japan Agency for Marine-Earth Science and Technology (JAMSTEC), Japan
Di Cai,
Tongji University, China

*CORRESPONDENCE
Valérie Chavagnac
valerie.chavagnac@get.omp.eu

RECEIVED 30 September 2023
ACCEPTED 30 September 2024
PUBLISHED 04 November 2024

CITATION
Chavagnac V, Destrigneville C, Boulart C, Taillandier V, Vigier N, Guieu C and Bonnet S (2024) Impact of submarine volcanic versus hydrothermal activity onto the strontium and lithium isotopic signatures of the water column (TONGA).
Front. Mar. Sci. 11:1304930.
doi: 10.3389/fmars.2024.1304930

Impact of submarine volcanic versus hydrothermal activity onto the strontium and lithium isotopic signatures of the water column (TONGA)

Valérie Chavagnac[1]*, Christine Destrigneville[1], Cédric Boulart[2], Vincent Taillandier[3], Nathalie Vigier[3], Cecile Guieu[3] and Sophie Bonnet[4]

[1]Géosciences Environnement Toulouse, GET UMR5563, CNRS/UPS/IRD/CNES, University of Toulouse, Toulouse, France, [2]Station Biologique de Roscoff, EDYCO – CHIMAR UMR7144, Roscoff, France, [3]Laboratoire d'Océanographie de Villefranche (LOV), Sorbonne Université/CNRS/Institut de la mer de Villefranche, Villefranche-sur-mer, France, [4]Institut Méditerranéen d'Océanologie (MIO), Aix Marseille Université/Université de Toulon/CNRS/IRD, Marseille, France

During the TONGA cruise (2019), seawater samples were collected to assess the effect of volcanic eruption versus submarine hydrothermal system on the water column. For this purpose, two locations were investigated, the first one located directly under the influence of the New Late'iki island (eruption in October 2019), and the second one showing ongoing submarine hydrothermal activity. At both locations, the total strontium (TSr) and lithium (TLi) concentrations vary between 94.4 and 152.3 µmol/L and 13.2 and 203.5 µmol/L, respectively. When combined, TSr and TLi concentrations of all samples in the water column are higher than those of the oligotrophic water. Both volcanic eruption and submarine hydrothermal activity (e.g. volcanic ashes, particles, gas condensate) can deliver substantial amount of TSr and TLi to the water column. The distribution of TSr versus TLi evidences linear trends either with a negative or positive slope. The negative correlation is observed in the water column at both sites, directly under the influence of the eruption and in the vicinity of the volcano with hydrothermal activity. The positive TSr versus TLi correlation is observed at site under submarine hydrothermal influence and is in line with black smokers related hydrothermal plumes. The $^{87}Sr/^{86}Sr$ ratios vary between 0.709147 and 0.709210 and δ^7Li values vary between +10.1 and +37.6 ‰. While 92% of the measured $^{87}Sr/^{86}Sr$ ratios are in line with the mean value of oligotrophic waters, once combined with the δ^7Li values, only 20% of them remains within this field. The wide range of δ^7Li values decreases from sea-surface down to ~140 mbsl, before increasing at greater depth, while defining different linear trend according to the dissolved inorganic carbon concentrations. The variability of δ^7Li values reflect hydrothermal contribution, mineral–seawater interaction and potentially biology–environment interaction. In the particular geological setting of the study, where both hydrothermal and volcanic activities were at play, disentangling both contributions on water column implies a combined use of elemental and isotopic signatures of Sr and Li tracers.

KEYWORDS

lithium isotopes, strontium, hydrothermalism, volcanic eruption, TONGA

1 Introduction

Along the 2,500 km long Tofua-Kermadec Arc in the Western Tropical South Pacific (WTSP), numerous submarine volcanoes have been identified using bathymetric map of the seafloor whereby only a few of them have their summit crossing sea level. This region is magmatically very active with about 77 volcanic eruptions which have been reported since the 18th century along the Tongan section alone (Global Volcanism Program, 2019). A significant number of powerful volcanic eruptions have taken place leading to hazardous phenomena via pyroclastic and explosive eruptions, air pollution of asphyxiant gases, and lava flows, stimulating the scientific communities to better explore and characterize submerged volcanoes and their associated hydrothermal system as well as their potential effect on environmental conditions for human health, ocean ecosystem and climate change (Stewart et al., 2022 among others). Trace elements such as iron, zinc, copper among others, derived from hydrothermal activity, are clearly identified as a main source of micronutrient to the water column with potential impact on the development and thriving of marine ecosystems on a global scale and at different water depth (German et al., 2016 for a review). For example, Bonnet et al. (2017), Guieu et al. (2018) and Tilliette et al. (2022) showed that a shallow submarine hydrothermal source was needed to provide the necessary dissolved iron level to maintain a high N_2-fixation rate, leading to increased primary production and carbon export (Bonnet et al., 2023).

In this area and on 14th October 2019, a powerful surtseyan volcanic eruption started nearby the Vava'u island and lasted until 30th of October. This event led to the formation of 21 000 m^2 New Late'iki island which was eroded by wave action within a few weeks and submerged by 14th December 2019 (Plank et al., 2020). During submarine volcanic event, different sources of material such as volcanic ash particles, hydrothermal fluids, gas condensates and salt precipitates, can be delivered to the hydrosphere modifying at different water depth seawater chemical composition, and therefore the living environment of marine ecosystems. The TONGA cruise which took place aboard the R.V. *L'Atalante* between 31st October and 5th December 2019, provided ideal temporal conditions to better constrain the dispersion of submarine shallow hydrothermal/volcanic supply to the water column. One of the objectives of the cruise was to constrain the impact of shallow hydrothermal supply on biogeochemical cycles, trace element content and dispersion in the water column and planktonic communities. For this purpose, two sites were investigated. The first one is directly under the influence of the New Late'iki island, and the second one (Volcano 1) showed in the early 2000s a significant hydrothermal activity (Stoffers et al., 2003; Massoth et al., 2007) that is still ongoing (Bonnet et al., 2023).

Here, we address the fate of volcanic-related emissions which can impact the water column nearby while we assess the detection and influence of hydrothermal-derived element supply from Volcano 1 on the surrounding seawater environment. The present study is entirely based on the chemical and isotopic signatures of water column samples collected at both sites. We selected two elements of interest, namely Strontium (Sr) and Lithium (Li). We report here total dissolved Sr (TSr) and Li (TLi). Their isotopic signatures are distinct in hydrothermal and marine environments, and they have both been applied in carbonate sedimentary archives to better reconstruct past carbon cycle variations (Misra and Froelich, 2012; Albarède et al., 1981; Palmer and Edmond, 1989; Vance et al., 2009; Millot et al., 2010a,b; Tomascak et al., 2016). Indeed, marine calcifiers form their carbonate shell from seawater-derived element pool which may contain the contribution of external sources, such as volcanic and/or hydrothermal ones. The comparison between the two selected sites may contribute in disentangling and fingerprinting geochemical features associated to each geological process, thus providing ideal isotopic tool to detect both processes in sedimentary archive over the Earth geological time-scale.

2 Materials and methods

2.1 Study area and sample collection

The studied area is located in the WTSP, nearby the Tonga-Kermadec subduction zone, along the Tofua-Kermadec arc (Figure 1A). Sample collection was carried out during the TONGA cruise which took place aboard the R.V. *L'Atalante* between 31st October and 5th December 2019. A 6,100 km long transect has been realized starting from New Caledonia within the Melanesian Waters, crossing the Tonga-Kermadec arc and entering the South Pacific gyre (GEOTRACE GPpr14; Guieu and Bonnet, 2019). The two locations of our study are Simone (19°24'S and 175° 03'W), just 10 nautical miles south from the New Late'iki island and Volcano 1 (21°09'S and 175°45'W) as shown on Figure 1A.

Simone is a submerged volcano, which is barely known about its morphology and lithology, thus far (Figure 1B). Volcano 1 is a stratovolcano located on the southern branch of the Tonga back-arc in the Lau Basin (Figures 1A, C). It has been extensively studied through CTD cast operations and direct observations via remotely operated vehicle dives (Stoffers et al., 2003; 2006; Massoth et al., 2007; Lupton et al., 2008). Volcano 1 displays an oval caldera (7 km long and 4.5 km wide) with a seafloor at 450 mbsl and two well-preserved scoria cones (Stoffers et al., 2003; 2006). At Volcano 1, the water column is strongly affected by submarine hydrothermal emissions as supported by multi-beam echo-sounder image evidencing fluid and gas hydrothermal emission rising up from caldera seafloor up to sub-surface (Figure 1D; Bonnet et al., 2023).

Vertical oceanographic profiles and seawater samples were collected at every station of the TONGA cruise. However, samples of interest for this study were only collected at a few casts located in the vicinity of the two sites (listed in Table 1). For all of these casts, a conventional 12 Niskin bottles rosette frame was deployed together with a Sea-bird SBE 9+ underwater unit equipped with a suite of *in-situ* physico-chemical sensors, namely two turbidimeters (Seapoint Turbidity Meters), one pH sensor (AMT GmBH) and one Eh sensor (AMT GmBH). Raw sensor data were processed into quality-controlled profiles at the vertical resolution of 1 mbsl as detailed in Taillandier et al. (2018). Seawater samples were not filtered aboard the research vessel prior to onshore chemical and isotopic analyses and were kept at 4°C until

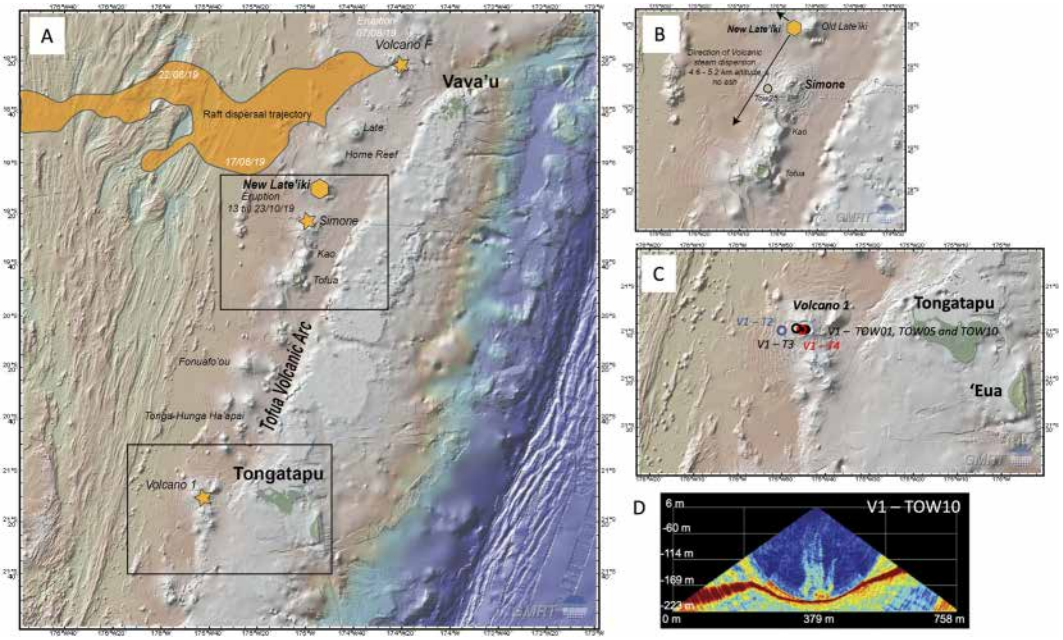

FIGURE 1
(A) Bathymetric map of the studied area in the WTSP (GMRT; Ryan et al., 2009). We report the location of Simone and Volcano 1 sites which are investigated here. The map also reports the locations of submarine volcanoes with their names. Two additional submarine volcanoes erupted recently, namely Volcano F which took place on August 2019 (Brandl et al., 2020) and led to a two-time Manhattan size pumice-raft which drifted away from its source over time, and the Hunga Tonga-Hunga Ha'apai volcano which erupted extremely violently on 15th January 2022 (Bernath et al., 2023). **(B)** Bathymetric map at the Simone location on which we report the location of S – TOW25 cast. We also report the direction of volcanic steam dispersion (Plank et al., 2020). **(C)** Bathymetric map at the Volcano 1 on which we report the location of each cast performed there. **(D)** Multibeam echo-sounder image performed at Volcano 1 just above the hydrothermal emissions at the caldera seafloor (modified from Bonnet et al., 2023).

aliquoting. CTD data were converted and processed using the SBE Data Processing software following Seabird recommendation for data corrections. Data from pH, Eh and turbidity sensors were averaged every 5 sec and outliers were removed using the median absolute deviation. All sensor data were processed using a R-based routine. All CTD casts were performed from onboard operation, without the involvement of submarine vehicle.

At the Simone site, the *in-situ* physico-chemical sensor package detected a turbidity layer below 190 mbsl i.e., seawater column investigation on the western flank of the volcano to the seafloor (~1200 mbsl) (Supplementary Figure S1). However, this feature was not associated to any hydrothermal-related physico-chemical anomalies (pH, Eh, temperature, salinity; Guieu and Bonnet, 2019) although acoustic anomalies likely attributed to hydrothermal activity were recorded. One CTD cast named "TOW25 Volcano2 St10 T2" was carried out enabling the collection of 4 samples (Table 1). During the cruise, the full sample name ensures its reference tracking within any database for analyses results that have been obtained on each sample. For clarity in the following sections, we will label this cast S–TOW25.

At Volcano 1 site, the full package of sensors enabled the detection of hydrothermal contribution to the water column at ~170 mbsl as evidenced by anomalies in temperature, salinity, turbidity, pH and Eh values (Bonnet et al., 2023; Figure 1D; Supplementary Figures S2, S3). This is in line with previous operations at this site by Massoth et al. (2007). For our study, Niskin bottles were fired during upward casts at different water depth in the water column where chemical and physical anomalies were detected. Three CTD casts were performed in the Volcano 1 caldera, namely "Station 5 TOW10 Panamax", "V1 CTD01 TOW01", and "TOW05 Volcano 1" between sea-surface and 200 mbsl collecting 26 seawater samples (Figure 1C). Additionally, three CTD casts (16 samples in total) were carried out along a westward transect covering a 17 km distance i.e., "Station 5 CTD15 V1 - T2", "CTD18 St5 V1 T3" and "St5 V1 TOW14 T4" (Figure 1C). For clarity in the following sections, we will label each cast at Volcano 1 as V1–TOW10, V1–TOW 01, and V1–TOW05 and each cast along a westward transect V1-T2, V1-T3 and V1-T4, respectively. Notwithstanding V1–T2 cast is located the furthest away from Volcano 1 and V1–T4 cast the closest.

2.2 Elemental and isotopic analysis

Water samples for dissolved methane (CH_4) analysis were taken from the Niskin bottles into precleaned and flushed 20 ml headspace glass vials and processed straight after the CTD-rosette was brought back on deck. The method of analysis was based on headspace extraction followed by gas chromatography analysis using a Shimadzu GC-BID coupled to a Shimadzu HS-20 headspace sampler. The detection threshold of this method is 0.2 nmol for dissolved CH_4, and variation between duplicates was 5% (Bonnet et al., 2023).

TABLE 1 Measured TLi and TSr elemental and isotopic signatures of water samples collected during the TONGA cruise.

Station	date	Depth (mbsl)	T (°C)	Salinity (PSU)	Eh (mV)	pH	TSr (µmol/L)	$^{87}Sr/^{86}Sr$	±2sE	TLi (µmol/L)	$\delta^{7}Li+$ (‰)	CH_4 (nmol/L)	DIC (µmol/L)
V1 CTD01 TOW01	09/ 11/ 2019	15	24.88	35.20	358	7.85	109.9	n.d.	n.d.	n.d.	n.d.	3.3	2033
V1 - TOW01		16	24.87	35.20	358	7.85	100.8	0.709178	0.000004	124.9	n.d.	0.5	1929
Latitude : 21.152 S		28	24.87	35.21	350	7.86	111.5	0.709205	0.000004	126.4	10.1	5.6	2119
Longitude : 175.741W		35	24.69	35.22	353	7.86	113.2	0.709205	0.000004	123.4	33.0	n.d.	2247
		45	24.51	35.23	367	7.86	121.3	0.709179	0.000003	107.2	29.3	2.6	2051
		54	24.45	35.24	372	7.86	109.9	0.709170	0.000004	128.6	32.3	1.7	n.d.
		63	24.25	35.26	372	7.86	112.2	0.709172	0.000004	119.8	36.0	23.6	2003
		75	23.93	35.29	385	7.87	99.2	n.d.	n.d.	131.8	n.d.	n.d.	2026
		77	23.92	35.29	381	7.87	126.0	0.709193	0.000004	203.5	27.6	12.0	n.d.
		106	23.02	35.37	441	7.88	120.4	0.709175	0.000004	146.8	n.d.	104.1	2048
		125	22.76	35.42	465	7.89	115.8	0.709168	0.000004	142.1	20.2	6.2	2073
		150	22.50	35.50	513	7.89	109.4	0.709165	0.000004	112.2	31.0	40.7	2296
TOW05 Volcano 1	09/ 11/ 2019	33	24.87	35.21	313	7.83	99.5	0.709166	0.000004	95.7	30.8	5.7	2048
V1 - TOW05		45	24.52	35.23	324	7.83	125.9	0.709171	0.000004	61.3	28.7	1.0	2008
Latitude: 21.155 S		63	24.27	35.25	343	7.84	152.3	0.709185	0.000004	n.d.	36.0	n.d.	2064
Longitude : 175.746W		94	23.30	35.33	417	7.83	109.9	0.709166	0.000004	64.7	n.d.	9.8	2048
		95	23.48	35.32	418	7.83	118.0	0.709183	0.000004	18.8	n.d.	1.9	n.d.
		97	23.37	35.33	424	7.83	113.5	0.709161	0.000004	79.6	28.7	5.7	2010
		105	23.21	35.36	418	7.83	119.0	0.709186	0.000004	n.d.	24.3	n.d.	n.d.
Station 5 TOW10 Panamax	11/ 11/ 2019	14	25.60	35.23	373	7.76	97.9	0.70919	0.000004	26.2	35.0	3.8	2350

(Continued)

10.3389/fmars.2024.1304930

TABLE 1 Continued

Station	date	Depth (mbsl)	T (°C)	Salinity (PSU)	Eh (mV)	pH	TSr (µmol/L)	$^{87}Sr/^{86}Sr$	±2sE	TLi (µmol/L)	$\delta^{7}Li+$ (‰)	CH_4 (nmol/L)	DIC (µmol/L)
V1 - TOW10		66	24.36	35.22	425	7.75	99.1	0.709179	0.000004	n.d.	27.0	9.8	1914
Latitude : 21.154 S		89	23.55	35.27	488	7.73	95.9	0.709189	0.000004	56.1	29.8	26.8	2845
Longitude : 175.745W		118	22.94	35.38	532	7.72	94.4	0.709165	0.000003	n.d.	26.6	3.8	2233
		152	22.07	35.57	591	7.71	118.5	0.709166	0.000004	115.8	32.0	44.5	2162
		177	21.54	35.64	607	7.67	112.2	0.70919	0.000004	45.8	32.2	2.6	2188
		194	21.47	35.65	563	7.63	102.2	0.709147	0.000004	38.7	24.8	16.2	2222
Station5 CTD15 V1-T2	12/ 11/ 2019	150	22.52	35.58	n.m.	n.m.	126.5	0.709199	0.000003	67.8	37.3	9.7	1977
V1 - T2		160	22.22	35.65	n.m.	n.m.	118.9	0.709179	0.000004	46.9	37.6	5.4	2013
Latitude : 21.159 S		178	21.74	35.66	n.m.	n.m.	109.2	0.709186	0.000005	78.2	32.3	2.1	2210
Longitude : 175.842 W		190	21.55	35.68	n.m.	n.m.	125.7	0.709187	0.000004	60.6	24.8	4.8	n.d.
CTD18 St5 V1 T3	13/ 11/ 2019	169	21.79	35.65	n.m.	n.m.	121.0	0.709197	0.000004	44.0	33.1	n.d.	2141
V1 - T3		181	21.58	35.64	n.m.	n.m.	119.5	0.709204	0.000004	55.2	28.6	n.d.	2094
Latitude : 21.155 S		190	21.30	35.66	n.m.	n.m.	116.0	0.709169	0.000004	76.5	n.d.	2.2	2048
Longitude : 175.762W		199	21.07	35.67	n.m.	n.m.	108.4	0.709183	0.000004	45.5	34.6	n.d.	2119
St5 V1 TOW14 T4	13/ 11/ 2019	70	24.14	35.38	450	7.75	99.0	n.d.	n.d.	111.4	n.d.	n.d.	2483
V1 - T4		96	23.62	35.38	454	7.73	103.7	n.d.	n.d.	65.6	n.d.	14.8	2195
Latitude : 21.155 S		161	21.98	35.39	535	7.73	102.4	n.d.	n.d.	72.0	n.d.	1.7	2297
Longitude : 175.751W		174	21.68	35.62	536	7.72	95.3	n.d.	n.d.	77.8	n.d.	5.9	2330

(Continued)

10.3389/fmars.2024.1304930

10.3389/fmars.2024.1304930

TABLE 1 Continued

Station	date	Depth (mbsl)	T (°C)	Salinity (PSU)	Eh (mV)	pH	TSr (µmol/L)	$^{87}Sr/^{86}Sr$	±2sE	TLi (µmol/L)	δ^7Li+ (‰)	CH_4 (nmol/L)	DIC (µmol/L)
		188	21.14	35.66	591	7.72	105.5	n.d.	n.d.	60.7	n.d.	5.5	2564
		195	20.94	35.67	618	7.72	107.0	n.d.	n.d.	47.0	n.d.	11.8	2281
		221	20.08	35.68	690	7.71	113.2	n.d.	n.d.	13.2	n.d.	3.1	2363
		260	19.41	35.64	761	7.71	99.6	n.d.	n.d.	87.0	n.d.	n.d.	2309
TOW25 Volcano2 St10 T2	24/11/2019	180	21.85	35.75	n.m.	n.m.	132.0	0.709158	0.000004	34.6	25.4	n.d.	n.d.
S - TOW25		800	5.31	34.36	n.m.	n.m.	112.7	0.70921	0.000004	53.9	27.0	n.d.	n.d.
Latitude: 19.416 S		870	4.82	34.39	n.m.	n.m.	132.4	0.709189	0.000004	43.8	32.1	n.d.	n.d.
Longitude : 175.052 W		950	4.37	34.40	n.m.	n.m.	140.1	0.709183	0.000004	17.2	n.d.	n.d.	n.d.

Environmental parameters measured *in-situ* i.e., temperature (°C), salinity (PSU), Eh (mV), pH are also reported. Onshore dissolved methane (CH_4, nmol/L) and DIC (µmol/L) concentrations are reported. n.d., not determined; n.m., not measured.

The TSr and TLi concentrations were measured by an inductively coupled plasma atomic emission spectrometer (ICP-AES) Horiba Ultima instrument at the Geosciences Environnement Toulouse laboratory. The instrument was calibrated with IAPSO seawater standard (OSIL Ltd., United Kingdom) doped with a prepared Li and Sr mono-elemental solution following the protocol described in Artigue et al. (2022). The IAPSO calibration curve was composed of one blank solution (Milli-Q water) and 6 solutions corresponding to a concentration range of 0 to 896.1 µmol/L for Li and 0 to 239.3 µmol/L for Sr. For TLi and TSr concentrations, raw seawater samples were doped with the same prepared dissolved Li and Sr mono-elemental solutions of known concentrations and with the same quantity. All samples were void of any particles by visual inspection. For each seawater sample, the TSr and TLi concentrations were quantified by the method of standard addition. The analytical precision was better than 2%. The limit of detection (3*SD) is determined by 10 consecutive analysis of Milli-Q water at 0.3 µmol/L for TLi and 0.01 µmol/L for TSr.

For the isotopic measurements, all seawater samples were treated in clean laboratory at the Geosciences Environnement Toulouse laboratory, to isolate via conventional liquid chromatography the two elements of interest from the heavily charged matrix. TSr was isolated using Sr-Spec resin (Eichrom, United States) using the protocol described in Pin et al. (2014) while TLi was isolated using two back-to-back ion exchange columns made of AGW-X12 200–400 mesh cation resin bed and eluted with 1N HCl based and adapted on the James and Palmer (2000) protocol.

The $^{87}Sr/^{86}Sr$ and $^{7}Li/^{6}Li$ isotopic ratios were measured with a Thermo Fisher Triton +, namely Thermal Ionisation Mass Spectrometer located at the Observatoire Midi-Pyrénées following the protocol described in Artigue et al. (2022). They were determined as the average values of 200 measurements of ion intensities following a static multi-collection mode. After purification in the clean laboratory, the TSr fraction was put back in solution with 1.5 µL mixture of 1/6 HPO_4 0.02N and 5/6 HCl 1N, loaded and dried down on a tungsten filament at 1 A. The $^{87}Sr/^{86}Sr$ ratios were corrected for mass fractionation based on the normalization value of $^{86}Sr/^{88}Sr$ ratio at 0.1194. The repeated measurements of the NBS 987 standard gave a mean value of 0.710260 ± 0.000015 (2SD; n = 8; 2SE = 0.000005). For each sample, the mean measured $^{87}Sr/^{86}Sr$ ratio was adjusted to the recommended value of the NBS 987 at 0.710250 i.e., a correction of -0.000010. Regarding the $^{7}Li/^{6}Li$ isotopic ratios, each purified TLi fraction were taken up in 3 µL of freshly made 0.15 N H_3PO_4, of which 1.5 µL was loaded on a degassed refined rhenium filament together with additional 1 µL of 0.15 N H_3PO_4. The sample was slowly dried down at 0.8 A filament current, then heated up to 2.4 A until phosphoric acid fumes were driven off, and then flashed at 2.8 A. During isotopic measurement, the current of the ionization filament was raised to ~2 A to reach a pyrometer temperature of ~1210–1220°C whereas the evaporation filament was increased to ~0.7–0.9 A until a stable ^{7}Li beam of ~5 V was reached. The repeated measurements of the IRMM-16 standard (Li_2CO_3) gave a mean value of 12.086 ± 0.016 (2SD; n = 42) in line with the reported value of 12.087 ± 0.015 (2SD; n = 33) in Artigue et al. (2022). The $^{7}Li/^{6}Li$ isotopic ratios of all samples are reported as δ^7Li ‰ notation relative to the IRMM-16 standard. The internal and external precision are 0.23 ‰ (2SE; n = 42) and 1.35 ‰

(2SD; n = 42), respectively. Seawater δ^7Li value is obtained using IAPSO seawater standard which is at +30.8 ± 0.1 ‰ (2SE, with external precision ≤ 1 ‰, Rosner et al., 2007).

3 Results

TLi and TSr elemental and isotopic signatures together with environmental parameters measured *in-situ* and dissolved CH_4 concentrations are reported in Table 1 for both sites. TSr and TLi elemental and isotopic signatures are represented as depth profiles in Figure 2 for Volcano 1. No TLi and TSr isotopic signatures are available for V1–T4.

3.1 Environmental parameters at Simone and volcano 1 sites

Depth profile of environmental parameters collected during CTD casts are reported in the Supplementary Materials for both sites (water depth reported as hydrostatic pressure). Complementary data such as trace metal concentrations (dissolved iron i.e., DFe), active acoustic data and turbulence among others are available in Tilliette et al. (2022), Bonnet et al. (2023) and Guieu et al. (2023).

Based on the distribution of the water properties recorded during the TONGA cruise, Tilliette et al. (2022) identified the different water masses present in the vicinity of the two volcanoes, expanding also regionally along the whole transect with roughly same vertical display. At these sites, the surface layer was well mixed in the first 30-50 mbsl and marked by high temperatures progressively decreasing with depth. Just below, a shallow salinity maximum identified the Subtropical Underwater (STUW); it was encountered between 150 and 350 mbsl at the two sites. Underneath, waters that make up the thermocline, so-called the Western South Pacific Central Water (WSPCW), extended down to 600 mbsl. Two water masses were identified at greater depth, the low salinity and high dissolved oxygen Antarctic Intermediate water (AAIW) down to 1300 mbsl, and below, the low dissolved oxygen and high nitrate Pacific Deep Water (PDW). This distribution shapes the water column with marked thermohaline gradients at their interfaces; in particular, the shallow hydrothermal activity encountered at the two sites was located inside STUW and their plume could extend to the surface layer crossing the sharp haline interface at the top of STUW. Internal waves preferentially propagate along this interface, and eventually break as it has been observed in the lee of the Tonga arc during the cruise.

At the Simone volcano site, the *in-situ* physico-chemical sensor package detected a turbidity layer below 190 mbsl (Supplementary Figure S1, not sampled). The sampled station was located downstream on the western flank of the volcano with a seafloor at 1200 mbsl depth (cast labeled S–TOW25 hereinafter). This cast enabled the collection of 4 samples in two turbidity layers (Table 1). A shallow turbidity layer was encountered inside the STUW core between 260 and 310 mbsl. Most likely, this layer corresponds to the extension of the plume observed at the volcano site. A second turbidity layer was encountered deeper, between 830 and 950 mbsl, just below the AIW core. These two features were not associated with any hydrothermal-related physico-chemical anomalies (pH, Eh, T° C, salinity, oxygen, Supplementary Figure S1).

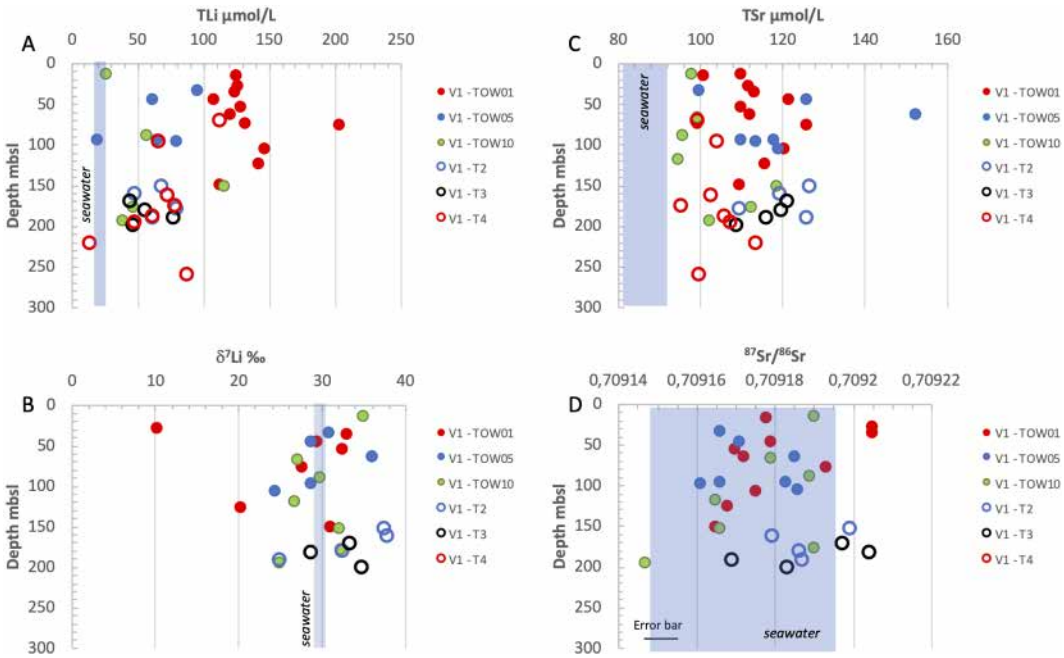

FIGURE 2
Depth profiles of TLi **(A)** and δ^7Li ‰ **(B)**, TSr **(C)** and $^{87}Sr/^{86}Sr$ in **(D)**, for Volcano 1 and transects samples. Blue boxes stand for seawater values (Leleu, 2017; Rosner et al., 2007; El Meknassi et al., 2018).

At Volcano 1, the full package of sensors enabled the detection of hydrothermal contribution to the water column at ~170 mbsl as evidenced by anomalies in temperature, salinity, turbidity, pH and Eh values (Bonnet et al., 2023; Figure 1D; Supplementary Figures S2–S6). This is in line with previous observations at this site by Massoth et al. (2007). The high-resolution transect above the caldera and the western flank of the Volcano 1 revealed a plume strongly maintained vertically below 140 mbsl by the salinity gradient of STUW, and horizontally by the orography of the caldera (reaching 100 mbsl). The extension of the plume on the flanks is limited at the km scale, with a thin turbidity layer centered at 200 mbsl depth (Figure S3). We also provide additional data of dissolved methane concentrations for Volcano 1 and transect casts. The concentrations vary between 0.5 and 104.1 nmol/L i.e., enriched dissolved CH_4 waters throughout the water column (Table 1; Supplementary Material S4-S6).

3.2 TLi elemental and isotopic signatures

TLi concentrations vary between 13.2 and 203.5 µmol/L and 90% of them are above oligotrophic 0.2 µm filtered water values at 24.6 µmol/L (Leleu, 2017) (Figure 2A). Overall, TLi concentrations in and around Volcano 1 cover the full variability range while those at Simone are at the lowest end of Volcano 1 values, reaching a maximum concentration of 53.0 µmol/L at 800 mbsl (Table 1). The three casts within the Volcano 1 caldera are located very close to one another but display strong TLi variability at the same water depth. Even if TLi concentrations at V1–TOW01 are the most enriched of all of them, away from the Volcano 1 caldera and along the transect the water mass between 150 and 200 mbsl is characterized by similar TLi concentrations, ranging between 44.0 and 78.2 µmol/L, but two to three times higher than oligotrophic water values. Nevertheless, we can still observe decreasing TLi concentrations with depth for V1–T4, the nearest cast to Volcano 1 caldera.

The δ^7Li values of all samples at both locations also display a large variability range at values lower, equal or higher than oligotrophic water of ~ +30.0 ‰ (IAPSO value at +30.8 ± 0.1‰, reproducibility <1 ‰; Rosner et al., 2007) i.e., between +10.1 and +37.6 ‰ (Figure 2B; Supplementary Figure S7). For the three casts performed within the submarine Volcano 1 caldera (V1–TOW01; V1–TOW05 and V1–TOW10), the δ^7Li values are progressively decreasing to first order from sea-surface (apart one exception) down to ~140 mbsl, before increasing abruptly at greater depth. At 140 mbsl, a strong shear zone within the water masses have been evidenced (Bonnet et al., 2023). Nevertheless, sea-surface waters can display the lowest δ^7Li value as well as one of the highest i.e., +10.1 ‰ vs. +35.0 ‰ (Table 1). There is no isotopic data for V1–T4. The water mass between 150 and 200 mbsl along the transect exhibits scattered δ^7Li values. At Simone, the δ^7Li values increase with depth from +25.4 up to +32.1 ‰ and fall within the same range as for those of Volcano 1.

3.3 TSr elemental and isotopic signatures

TSr concentrations vary between 94.4 and 152.3 µmol/L (Figure 2C), all above the oligotrophic 0.2 µm filtered water range of 80-90 µmol/L (El Meknassi et al., 2018). At Simone, TSr concentrations are at the higher end of the Volcano 1 ones, and vary between 112.7 and 140.1 µmol/L (Table 1). There, the highest TSr concentration is measured at 950 mbsl. For Volcano 1 caldera, no obvious trend is observed but the maximum concentration of 152.3 µmol/L is measured at ~64 mbsl. Along the westward transect, TSr concentrations vary within the same range as those of Volcano 1 caldera. Nevertheless, we observe increasing TSr concentrations of the water mass when moving westward from V1–T4 to V1–T2 (Figure 2C).

Figure 2D presents the variation of the $^{87}Sr/^{86}Sr$ ratios as depth profiles. The $^{87}Sr/^{86}Sr$ ratios vary between 0.709147 and 0.709210 with a mean value of 0.709181 ± 0.000014 (1SD; 2SE = 0.000006, n = 36) (Supplementary Figure S8). 92% of the measured $^{87}Sr/^{86}Sr$ ratios are within the 95% confidence interval of the average value of oligotrophic waters of 0.709172 ± 0.000023 (2SD; n = 84; El Meknassi et al., 2018). A recent value of seawater Sr isotopic signature highlights an identical average $^{87}Sr/^{86}Sr$ ratio at 0.709172 ± 0.000003 (North Deep Pacific seawater; 2SD, n = 6; Wakaki et al., 2017) but with a much smaller standard deviation. Considering respective numbers of Sr isotopic data in each study, their standard error on the average value are identical at 0.000003 (2SE).

4 Discussion

TSr and TLi are ideal tracers to track down sources contribution and to fingerprint water-rock interaction and processes at play (Huh et al., 1998; Brunskill et al., 2003; Davis et al., 2003; Barker et al., 2008; Vance et al., 2009; Millot et al., 2010b; Araoka et al., 2016; Chavagnac et al., 2018; Artigue et al., 2022). In the present study, the two selected sites are under the influence of different sources, meaning eruptive volcanism for Simone and submarine hydrothermalism for Volcano 1. Before considering both geological contexts, we observe clearly different behaviors between these two tracers based on the variability of their concentrations. Combining both TSr and TLi concentrations in Figure 3 points out that all samples are located outside the range of oligotrophic waters. Moreover, their variability defines a linear trend which has either a negative slope, especially at Simone, or a positive one. It remains to elucidate whether the observed trace element distributions reflect the two different and distinctive geological contexts, involving different processes and elemental sources. However, all transect casts nearby Volcano 1 influence display TSr and TLi concentrations mimicking those at Simone, questioning the dispersion of hydrothermal input in Volcano 1 vicinity.

Indeed at Volcano 1, the water column is strongly affected by submarine hydrothermal emissions as supported by multi-beam echo-sounder image evidencing fluid and gas hydrothermal emission rising up from caldera seafloor up to sub-surface (Figure 1D; Bonnet et al., 2023). At this location, water column environment is suboxic (low dissolved oxygen), slightly acidic (pH down to 6.5; Bonnet et al., 2023), enriched in dissolved methane concentrations (Table 1) and high CO_2 content (high DIC concentrations, Table 1), with extreme and abrupt concentration variation throughout the water column (Supplementary Material S4–S6). Moreover, Tilliette et al. (2022) measured DFe

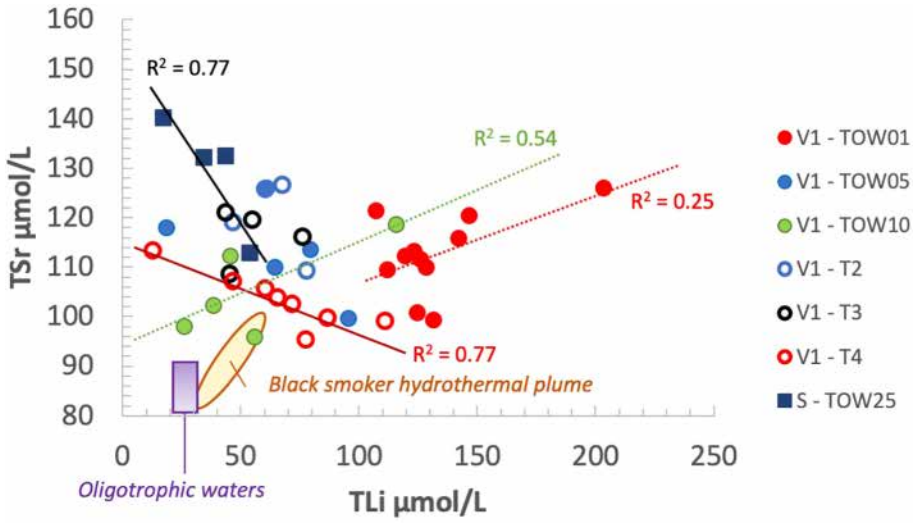

FIGURE 3
TSr vs TLi concentration plot of collected samples in comparison to oligotrophic waters (Leleu, 2017; El Meknassi et al., 2018) and black smoker hydrothermal plume (Artigue et al., 2022). Linear trends with R^2 values are reported for S–TOW25, V1–T4, V1–TOW01 and V1–TOW10.

concentrations of water column samples and found high DFe hydrothermal input from caldera seafloor to sub-surface water (3-5 times higher than typical oligotrophic DFe concentrations). Their datasets argued for a weak hydrothermal plume dispersion, whereby only a few % of initial hydrothermal DFe supply is maintained as dissolved form within the photic zone when moving westward from Volcano 1 caldera. To explain this DFe distribution pattern, three main processes were invoked such as mineral precipitation, trace element scavenging and to a lesser extend biological uptake; all of them potentially affecting the TSr and TLi elemental and isotopic composition distribution studied here.

4.1 Simone site

Simone site is under the direct influence of a volcanic eruption of surtseyan style which is characterized by emission of volcanic plumes rich in water vapor, condensed water and fine volcanic ash and associated water-rock interaction processes. Volcanic material can be transported hundreds of kilometres away from the source either in the marine realm (Newland et al., 2022; Clare et al., 2023) or in the atmosphere as a 4.6 to 5.2 km altitude steam plume has been reported during this volcanic eruption leading to New Late'iki island formation (Global Volcanism Program, 2019). Both processes can deliver volcanic materials supplying additional Li and Sr to the environment, and leading to higher concentrations in water column.

During volcanic eruption, the volcanic plume is strongly enriched in Li because the partition coefficient for alkali element such as Li is well above 1000 during magmatic vapor–magma interaction (Lowenstern et al., 2012). Moreover, the volcanic plume is also enriched in gases mainly composed of CO_2, H_2O, SO_2 among others (Symonds et al., 1994; Aiuppa et al., 2009) and is the place of many processes leading to little acidic droplets formation composed of HCl, HF, H_2SO_4 (Symonds et al., 1988; Zhu et al., 2020) and to salt precipitation on ash surfaces (Rose, 1977; Oppenheimer, 2003; Delmelle et al., 2007, 2018). The occurrence of acidic droplets enables local dissolution of particle ashes in line with a few dissolution holes observed on microscopic images of lithogenic particles collected in the water column at S–TOW25 location (Tilliette et al., 2023a). Indeed, lithogenic particles display essentially angular, clean and smooth surfaces pointing out limited influence of particle dissolution within the water column as well as particle freshness i.e., lack of remobilization and resuspension of old seafloor particle in the water column (Tilliette et al., 2023a). Particles from sea-surface sank progressively vertically and are advected horizontally (Tilliette et al., 2023a). Colombier et al. (2019) characterized that extensive salt precipitation as NaCl and $CaSO_4$ on surface particle occurs during surtseyan volcanic eruption, taking the Hunga Tonga - Hunga Ha'apai tuff cone as a site study (this volcano is part of the Tofua volcanic arc (Figure 1A), just north of Volcano 1). The dissolution of these salts (Stewart et al., 2020) leads to Li and Sr supplies in the water column as Li is known to be highly concentrated in brine (Garcia et al., 2020) and Sr is enriched in $CaSO_4$ e.g., anhydrite such those found at black smoker hydrothermal field (1164 to 2218 ppm; Humphris and Bach, 2005). Thus, this process may explain why the TSr and TLi concentrations measured at Simone are higher than those of oligotrophic waters i.e., by a factor of two (Figure 3). Considering the Na/Li molar ratio of brines at 61 (Garcia et al., 2020), an increase of 25-30 µmol/L of Li in seawater would induce a global salinity (reported here as halite) increase of ~0.1 g/L. In addition, we observe a negative TSr vs. TLi linear trend (Figure 3). Chemical analyses of brine samples collected at the Ethiopian rift under the direct influence of tectonism and volcanism, also evidence negative Sr vs. Li correlation (Bekele and Schmerold, 2020). Even if the dissolution of these salts leads to higher TSr and TLi concentrations,

a different dissolution rate of Sr- and Li-bearing minerals i.e., anhydrite vs. halite, should induce distinctive TSr and TLi supply to the water column. Halite is highly soluble (Alkattan et al., 1997) and its dissolution would deliver Li which will be instantaneously diluted within the water column. Even if the TLi concentrations are similar to that of oligotrophic waters at Simone site, the δ^7Li values are significantly different near the surface from oligotrophic waters i.e., +25.4‰, increase with water depth and reach a value similar to oligotrophic water near the seafloor (Table 1). This δ^7Li shift towards lower value compared to oligotrophic water can potentially reflect the combined effect of brines dissolution and biological uptake. A potential contribution of brine is supported by their low δ^7Li values at +5.9 to +10.3 ‰ (Garcia et al., 2020), meaning that any contribution would lower the δ^7Li value of the solution. The second hypothesis is based on recent scientific outcomes from the studied area evidencing high primary productivity rate estimated up to 145 mmol C m^{-2} yr^{-1} at this location (Tilliette et al., 2023a), together with the increase of organic matter and calcium carbonate within the particle pool collected by sediment trap at 200 mbsl (Tilliette et al., 2023a). Marine carbonate organisms are very diverse. Preliminary studies have showed that mussel/oyster/clam, all having a calcium carbonate shell, are preferentially enriched in ^{7}Li i.e., higher δ^7Li values compared to that of their aqueous environment which shows consequently low δ^7Li values (Thibon et al., 2021). Thibon et al. (2021) showed that these marine carbonate calcifiers tend to accumulate Li proportionally to the Li concentration of their surrounding aqueous environment. Indeed, at the studied area, Vigier et al. (2022) showed that plankton is characterized by very high Li concentrations (10 to 120 µg/g dry weight) compared to any other marine carbonate calcifiers (≤1 µg/g dry weight; Thibon et al., 2021), suggesting therefore that Li concentration of seawater at this location should be very high, as we argue here. In case of mineral–water interaction, ^{6}Li is preferentially adsorbed onto particles (lithogenic particle), leading to isotopic fractionation evidenced by high δ^7Li values for the solution and low δ^7Li values for particle, such as smectite among others (Chan and Hein, 2007; Vigier et al., 2008; Araoka et al., 2016). Here, the δ^7Li values of collected samples are equal and lower to that of seawater within error, reflecting the absence of particle–seawater interaction.

Unlike Li, TSr concentrations are all above the range of oligotrophic waters along depth profile (Table 1). Considering anhydrite with a Sr concentration of 1164 to 2218 ppm (Humphris and Bach, 2005) as the potential source of Sr, a maximum 50 µmol/L increase of TSr in our sample compared to oligotrophic waters (80–90 µmol/L) is thermodynamically possible and would imply the dissolution of 1.9 to 3.7 g/L of anhydrite which is below the solubility of anhydrite in seawater characterized by 4.95 g/L and 25°C (values calculated from PHREEQC). This suggests that anhydrite dissolution is a feasible process in the geological context of Simone. Further investigation on volcanically derived anhydrite is needed to better constrain the dissolved amount of this mineral as the available Sr dataset on anhydrite is solely provided by hydrothermal environment. Nevertheless, the ^{87}Sr/^{86}Sr ratios fall within the range of oligotrophic ones, except at 800 mbsl. The least radiogenic ^{87}Sr/^{86}Sr ratio of 0.709158, is measured at 180 mbsl, and can signify a contribution from the dissolution of basaltic material i.e., ^{87}Sr/^{86}Sr = 0.703–0.704 (Escrig et al., 2012), especially as a dense nephelometric layer was detected between 260 and 310 mbsl (Guieu and Bonnet, 2019). This nephelometric layer can be related to volcanic material delivered to the water column by erosion processes of the New Late'iki island (Plank et al., 2020). Indeed, by 24th November 2019 i.e., date of sample collection at Simone, erosion processes were still in progress delivering a substantial amount of volcanic particles to the water column (Tilliette et al., 2023a). At greater water depth, ^{87}Sr/^{86}Sr ratios are linearly correlated to 1/TSr (R^2 = 0.99) as shown in Supplementary Figure S8, with a trend controlled by the most radiogenic ^{87}Sr/^{86}Sr ratio of 0.709210. The analyzed samples have been sampled within the nephelometric layer as shown in Supplementary Figure S1, indicating the occurrence of particles. Similar radiogenic ratios are also measured at Volcano 1 and along the transect away from Volcano 1. With the present dataset, we cannot propose a potential source for such Sr isotopic signatures (Table 1, Figure 2D).

4.2 Volcano 1 site

The TSr vs. TLi distribution defines two linear tendencies with either negative or positive slope (Figure 3). Away from the Volcano 1 and along the transect, the TSr vs. TLi concentrations show negative linear trends, as that observed at Simone. However, the slope value decreases gradually when getting closer to Volcano 1. Within Volcano 1 caldera, this negative slope is observed for V1–TOW05 but V1–TOW01 and V1–TOW10 casts show a positive linear trend. These observations clearly evidence a heterogeneous and complex environment within a submarine volcano caldera. Indeed, at Volcano 1, active hydrothermal activity has been identified at the caldera seafloor through direct observation of fluid emission in the early 2000s (Stoffers et al., 2006; Massoth et al., 2007). In 2019 during the TONGA cruise, this hydrothermal activity was still ongoing as evidenced by physico-chemical anomalies detected in the water column at similar seafloor location (Bonnet et al., 2023; Supplementary Material S4, Supplementary Material S5-S6). Strong hydrothermal input is also supported by the high dissolved methane concentrations measured at this location, as oligotrophic waters commonly exhibit low methane concentrations of ~0.5 nmol/L (Table 1). A positive linear correlation of TSr vs. TLi was previously evidenced at black smokers of the Lucky Strike hydrothermal field (LSHF, on the Mid-Atlantic ridge) based on the analyses of 0.2 µm filtered seawater samples collected up to 300 m above the seafloor covering the 1 km^2 hydrothermal field (Artigue et al., 2022). Artigue et al. (2022) interpreted this co-variation (similar positive slope as our study), as reflecting a hydrothermal contribution of up to 10% to the water column. At Volcano 1, the hydrothermal contribution would be much more important as the TSr and TLi concentrations are increased by 5–41% and 7–88%, respectively compared to oligotrophic water concentrations. High hydrothermal contribution is also highlighted by very high dissolved methane concentration up to 104.1 µmol/L measured within the Volcano 1 caldera, and to a lesser extend along the transect. The variation of

TSr and TLi concentrations according to their respective isotopic signatures i.e., $^{87}Sr/^{86}Sr$ ratios and δ^7Li values, respectively, do not define any clear linear relationship which would have reflected binary mixing, apart from V1-TOW01. For this cast and without surface seawater samples i.e., <35 mbsl, the Sr elemental and isotopic signatures of samples define a linear trend (R^2 = 0.74) suggesting mixing between oligotrophic water and an unradiogenic Sr isotopic source depleted in Sr compared to seawater (Supplementary Figure S8). Unfortunately, at Volcano 1, the seafloor hydrothermal fluids have not been characterized for their TSr and TLi elemental and isotopic signatures thus far, hindering further calculation to better constrain hydrothermal contribution to the water column. Nevertheless, information can be obtained from worldwide sites exhibiting similar geological setting. At submarine Niuatahi Volcano (174°W and 15.35°S, Tonga rear arc), Falkenberg et al. (2022) report the occurrence of different venting styles displaying acid-sulfate (clear) to black smoker (particle-bearing) hydrothermal fluids and encompassing fluid boiling to magmatic volatile influxes. This study points out the complexity and diversity of hydrothermal venting, unfortunately without Sr and Li dataset on fluids. Wilckens et al. (2019) characterized chemically and isotopically both styles of venting at similar geological setting further north at North Su and DESMOS volcanic back-arc. Unfiltered acid-sulfate hydrothermal fluids display Sr and Li concentrations at 59–87 µmol/L and 21-41 µmol/L for corresponding isotopic signatures at 0.7087 to 0.70902 and +17.2 to +30.1 ‰, respectively (Wilckens et al., 2019). Unlike acid-sulfate fluids, unfiltered black smoker ones from the same location exhibit contrasted and distinctive Sr and Li elemental and isotopic signatures. Indeed, all black smoker fluids are enriched in Sr (151–410 µmol/L) and Li (348–806 µmol/L) for isotopic signatures being closer to substratum values at 0.70444 to 0.70582 and +5.7 to +6.8 ‰, respectively (Wilckens et al., 2019). Furthermore, the 0.2 µm filtered LSHF black smoker fluids are characterized by Sr and Li concentrations at 76–139 µmol/L and 287–398 µmol/L, respectively, and $^{87}Sr/^{86}Sr$ ratios and δ^7Li values at 0.70383 to 0.70436 and +4.8 to +5.9 ‰, respectively (Leleu, 2017; Artigue et al., 2022). Thus, this shows that volcanic-arc hydrothermal systems (Li = 0.23 to 1.3 mmol/kg and δ^7Li = +4.3 to +7.2 ‰; Araoka et al., 2016) have similar chemical features as basalt-hosted black smokers on mid-ocean ridges (Artigue et al., 2022; Wilckens et al., 2019; among others). Taking these elemental and isotopic signatures into account, the $^{87}Sr/^{86}Sr$ vs. (1/TSr) trend observed for V01–TOW01 can potentially reflect the contribution of an acid-sulfate hydrothermal fluid but alone this source cannot explain the large variability observed here for all casts performed at and away from Volcano 1.

In Figure 4, we report the $^{87}Sr/^{86}Sr$ ratios vs. δ^7Li values for collected samples together with the domains of that ratio in the literature for oligotrophic waters, acid-sulfate fluids and black smokers. While 92% of the measured $^{87}Sr/^{86}Sr$ ratios are in line with the mean value of oligotrophic waters of 0.709172 ± 0.000023 (2SD; n = 84; El Meknassi et al., 2018), the δ^7Li values display a large variability at values lower, equal or higher than oligotrophic water at +30.8 ± 0.1 ‰ (Rosner et al., 2007) i.e., between +10.1 and +37.6 ‰. Once combined, only 20% of measured samples fit within the field of oligotrophic water signatures (Figure 4). Sr and Li isotope systematics are key tracers of source, and Li isotopes provide additional information on processes related to mineral–seawater interaction (Chan and Hein, 2007; Artigue et al., 2022) and biology–aqueous environment interaction (Vigier et al., 2015; Thibon et al., 2021; Vigier et al., 2022; Poet et al., 2023; Chen et al., 2023). In Figure 4, we observe the combined effects of sources and processes. Four samples exhibit $^{87}Sr/^{86}Sr$ ratios more radiogenic than oligotrophic waters. Previous studies such as Nonell et al. (2005) report $^{87}Sr/^{86}Sr$ ratios ranging between 0.7049 and 0.71008 on volcanic gas condensates at Vulcano Island (Italy). Thus, it is possible that a substantial amount of gas condensate with radiogenic Sr isotopic signatures is produced in Volcano 1 caldera, increasing $^{87}Sr/^{86}Sr$ ratios towards more radiogenic signatures than oligotrophic waters. The main feature of the remaining samples relies on the δ^7Li values and their variability. Lower ones (32% of all samples) compared to oligotrophic waters are in line with hydrothermal contribution while higher ones (52% of all samples) can fingerprint either mineral–seawater interaction or biology-seawater interaction as DFe distribution in the water column suggests mineral precipitation, trace element scavenging and biological uptake (Tilliette et al., 2022).

In Figure 5, we report the measured δ^7Li values according to the DIC concentrations acquired on the same water samples. For comparison we also report the measured values on foraminifera shells collected after culture experiments in solution at different DIC concentrations (Vigier et al., 2015). DIC concentration in seawater is ~2400 µmol/L. Three putative trends can be proposed. Trend 1 delineates decreasing DIC concentrations for higher δ^7Li values compared to seawater features i.e., samples collected along transect casts and sub-surface Volcano 1 samples (0-50 mbsl). This feature can signify either the effect of mineral–seawater interaction, as ^6Li is preferentially adsorbed on mineral surfaces (Chan and Hein, 2007; Vigier et al., 2008), leading to ^7Li enrichment in the water column (Artigue et al., 2022) or the phytoplankton–seawater interactions, as Vigier et al. (2022) showed that plankton at this location exhibit lower δ^7Li values than seawater, leading to high δ^7Li values in solution. Trend 2 is defined by decreasing DIC concentrations concomitantly to lower δ^7Li values compared to seawater. This is evidenced by samples of Volcano 1 collected between 50 and 150 mbsl. Seawater sampled at depths greater than 50 mbsl is enriched in dissolved iron concentrations by several orders of magnitude compared to oligotrophic waters [Figure 3 in Tilliette et al. (2022)] as well as in dissolved methane concentrations (Table 1), in line with submarine hydrothermal contribution. The latter is further supported by lower δ^7Li values compared to oligotrophic water, as any hydrothermal contribution whether of acid-sulfate or black smoker type would lower δ^7Li values of seawater, based on the reported δ^7Li values of Wilckens et al. (2019). Trend 3 displays lower DIC concentrations and δ^7Li values compared to oligotrophic waters, mimicking trend 2 but with a much steeper slope i.e., narrower range of DIC variability. While submarine hydrothermal source can provide substantial amount of macronutrient up to the euphotic zone to stimulate phytoplankton development, hence carbon export, modification of seawater chemical composition can at first stress phytoplankton community, inhibiting biological activity until aqueous environments return to more favorable

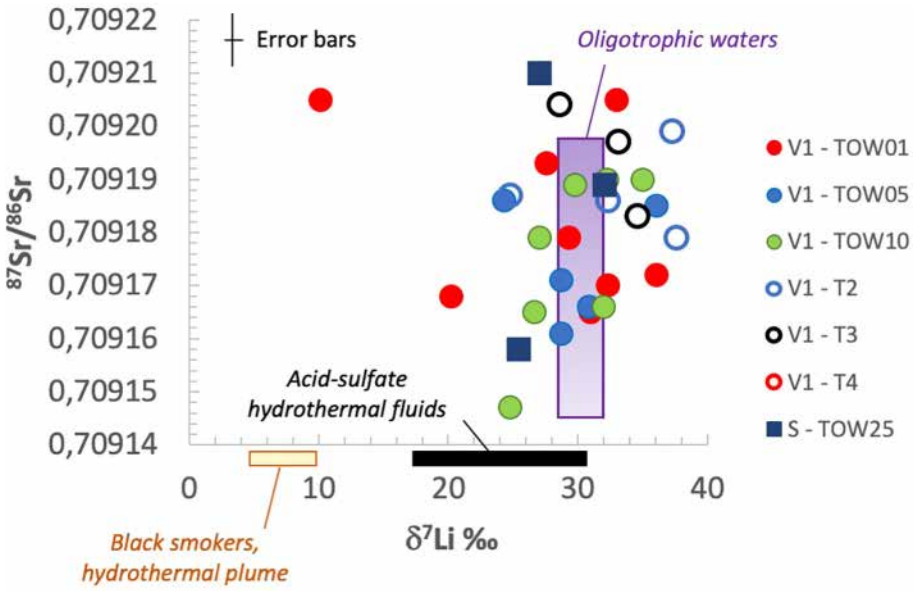

FIGURE 4
Binary diagram of δ^7Li values and $^{87}Sr/^{86}Sr$ ratios for collected samples in comparison to oligotrophic waters (Rosner et al., 2007), acid-sulfate hydrothermal fluids (Wilckens et al., 2019) and black smoker hydrothermal plume signatures (Artigue et al., 2022).

conditions. Using experimental minicosms operated during the TONGA cruise, Tilliette et al. (2023b) showed that production of thiol ligand by *Synechococcus* ecotypes enables binding of trace metals such as Cu, Cd, and Hg, leading to detoxification of the environment. As a consequence, phytoplankton growth i.e., enabling carbon export, can be delayed by several days, depending on the detoxification of the environment. Due to limited DIC and δ^7Li values, further scientific research is needed to assess the effect of biological activity onto Li elemental and isotope behavior in a context of high hydrothermal contribution. Overall, it is unfortunate that drifting conical sediment trap deployed at 200 mbsl within the caldera of Volcano 1 did not operate (Tilliette et al., 2023a), which would have helped us in characterizing particle chemistry and mineralogy as well as composition of the biogenic fraction. Meanwhile, the surtseyan volcanic eruption as well as hydrothermal systems can generate strong currents in the water column as a consequence of important heat supply in a cold environment (Dutay et al., 2004). Bonnet et al. (2023) identified a high-salinity water mass below surface waters, at the top of the permanent thermocline, which may have impacted the distribution of δ^7Li values according to depth (Figure 2B).

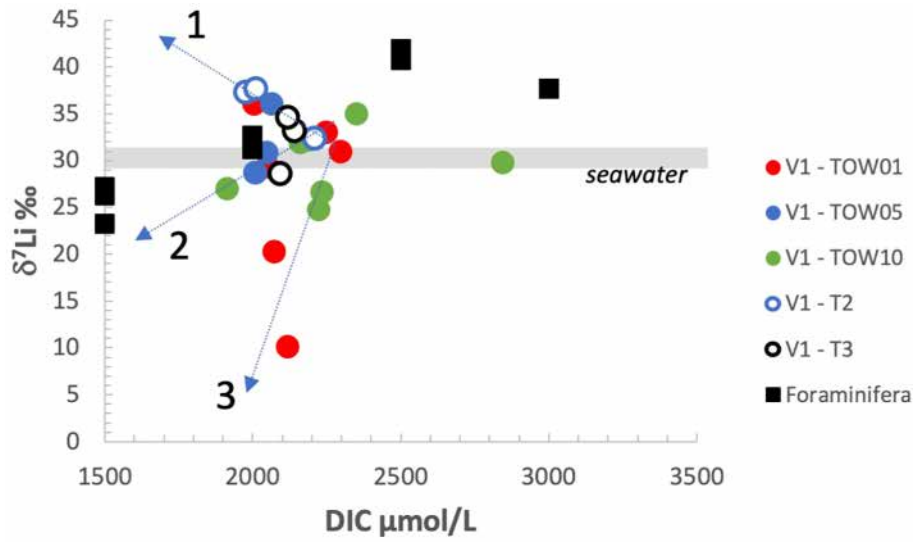

FIGURE 5
Binary diagram of Replacement TextLi values and DIC concentrations for collected samples. Measured δ^7Li values of foraminifera cultured in solution of various DIC concentrations are reported for comparison (Vigier et al., 2015). See the text for explanation of the three trends.

4.3 Effects of volcanic vs. hydrothermal contribution on water column

The effect of volcanism and hydrothermalism is evidenced by higher TSr and TLi concentrations of the water column compared to oligotrophic water ones. The volcanic contribution is expressed by high TSr and TLi concentrations due to the dissolution of different salts coating ash particles i.e., halite enriched in Li and anhydrite enriched in Sr. These supplies are directly linked to the eruptive style of volcanism. We observe this process at Simone site, directly under the influence of the New Late'iki eruption, and along the transect casts located ~150 km southwest of Simone. There, TSr concentrations decrease as TLi increases concomitantly. Unlike volcanic eruption, hydrothermalism provokes mutual increases of TSr and TLi in the water column. We observe this process in the Volcano 1 caldera at two out of three casts. When applying TSr and TLi isotopic systematics, the $^{87}Sr/^{86}Sr$ ratios vs. δ^7Li values point to different inputs as well as processes involving seawater interaction with particles and biological activity. In particular, this is evidenced by high δ^7Li values compared to oligotrophic waters at Volcano 1. Nonetheless, particles can be of different origin i.e., volcanic eruption ejects ashes while hydrothermalism leads to mineral formation within the mixing gradient between hydrothermal fluid and surrounding seawater. While processes can be similar, the minerals involved are distinctive in composition. They are either lithogenic in volcanic context, or polymetallic sulfides and oxyhydroxides in the case of hydrothermalism, leading to different isotopic fractionation when interacting with seawater. Alternatively, marine organisms rely on macro-nutrient supply to thrive. Submarine hydrothermal source provides a substantial amount of trace elements to seawater, among which some of them can stimulate primary productivity i.e., dissolved iron, while others, such as Hg or Cu can provoke the opposite, by inhibiting their development once their dissolved concentrations are too elevated. As a consequence, marine carbon export can be affected. Vigier et al. (2022) showed that plankton collected at hydrothermal setting is characterized by very high Li concentrations together with low δ^7Li values compared to seawater. In this particular setting where both volcanic and hydrothermal activities were at play, disentangling both contributions on water column required the combined use of elemental and isotopic signatures of several tracers, here Sr and Li.

5 Conclusion

The present study based on the TSr and TLi elemental and isotopic signatures of water column samples collected at Simone and Volcano 1 sites, reveals the contributions of volcanic and hydrothermal products to the surrounding environment. This is clearly evidenced by TSr and TLi concentrations higher than oligotrophic waters. Both volcanic eruption and submarine hydrothermal activity e.g., volcanic ashes, particles, gas condensate, etc., can deliver substantial amount of TSr and TLi to the water column.

On one side, volcanic eruption of surtseyan style is characterized by emission of volcanic plumes rich in water vapor, condensed water and fine volcanic ash and associated water-rock interaction processes. We observe a negative correlation between TSr and TLi in the water column at Simone and close to Volcano 1 that we propose to reflect differential dissolution rates of salt-coated ejected ashes since Sr and Li are associated to different minerals, anhydrite and halite respectively. Further analyses of ashes and Ca, sulphate and chloride concentrations in the water column need to be conducted to support this hypothesis. On the other side, hydrothermal supply at Volcano 1 leads to a positive TSr vs. TLi correlation, in line with black smoker related hydrothermal plume (Artigue et al., 2022).

When applying TSr and TLi isotopic systematics, the $^{87}Sr/^{86}Sr$ ratios vs. δ^7Li values point to different sources as well as processes involving seawater interaction with particles and/or biology. While 92% of the measured $^{87}Sr/^{86}Sr$ ratios are in line with the mean value of oligotrophic waters, only 20% of them remain within the field once combined with δ^7Li values. The δ^7Li values display a large variability i.e., between +10.1 and +37.6 ‰, decreasing linearly to first order from sea-surface down to 140 mbsl i.e., depth of water mass shear zone. The different linear trends defined between δ^7Li values and DIC concentrations highlight particle–seawater interaction, hydrothermal contribution and biology–seawater interaction.

When considering geological sedimentary archive, disentangling volcanic vs. hydrothermal contribution relies on combining different tracers among which one tracks down sources and another fingerprints water-rock interaction processes.

Data availability statement

The original contributions presented in the study are included in the article/Supplementary Material. Further inquiries can be directed to the corresponding author.

Author contributions

VC: Conceptualization, Formal analysis, Methodology, Validation, Writing – original draft, Writing – review & editing. CD: Writing – original draft, Writing – review & editing. CB: Data curation, Writing – original draft, Writing – review & editing. VT: Data curation, Formal analysis, Writing – review & editing. NV: Writing – original draft, Writing – review & editing. CG: Funding acquisition, Writing – original draft, Writing – review & editing. SB: Funding acquisition, Writing – original draft, Writing – review & editing.

Funding

The author(s) declare financial support was received for the research, authorship, and/or publication of this article. The ANR

-TONGA (ANR-18-CE01-0016) provided funding for all authors. In addition, the TONGA project and cruise was funded by the IR* Flotte Océanographique Française, the A-MIDeX of Aix-Marseille University, the LEFE-CYBER and GMMC program.

Acknowledgments

We are grateful to the IR* French Oceanographic Fleet and the crew of the R.V. L'Atalante which provided the technical support to carry out sample collection at sea during the oceanographic cruise TONGA. We acknowledge constructive comments from five reviewers and Johan Schijf.

Conflict of interest

The authors declare that the research was conducted in the absence of any commercial or financial relationships that could be construed as a potential conflict of interest.

Generative AI statement

The author(s) declare that no Generative AI was used in the creation of this manuscript.

Publisher's note

Supplementary material

The Supplementary Material for this article can be found online at: https://www.frontiersin.org/articles/10.3389/fmars.2024.1304930/full#supplementary-material

References

Aiuppa, A., Baker, D. R., and Webster, J. D. (2009). Halogens in volcanic systems. *Chem. Geology* 263, 1–18. doi: 10.1016/j.chemgeo.2008.10.005

Albarède, F., Michard, A., Minster, J. F., and Michard, G. (1981). $^{87}Sr/^{86}Sr$ ratios in hydrothermal waters and deposits from the East Pacific Rise at 21°N. *Earth Planetary Sci. Lett.* 55, 229–236. doi: 10.1016/0012-821X(81)90102-3

Alkattan, M., Oelkers, E. H., Dandurand, J.-L., and Schott, J. (1997). Experimental studies of halite dissolution kinetics, 1 The effect of saturation state and the presence of trace metals. *Chem. Geology* 137, 201–219. doi: 10.1016/S0009-2541(96)00164-7

Araoka, D., Nishio, Y., Gamo, T., Yamaoka, K., and Kawahata, H. (2016). Lithium isotopic systematics of submarine vent fluids from arc and back-arc hydrothermal systems in the western Pacific. *Geochemistry Geophysics Geosystems* 17, 3835–3853. doi: 10.1002/2016GC006355

Artigue, L., Chavagnac, V., Destrigneville, C., Ferron, B., and Cathalot, C. (2022). Tracking the lithium and strontium isotope signature of hydrothermal plume in the water column: A case study at the EMSO-azores deep-sea observatory. *Front. Environ. Chem.* 3. doi: 10.3389/fenvc.2022.784385

Barker, A. K., Coogan, L. A., Gillis, K. M., and Weis, D. (2008). Strontium Isotope Constraints on Fluid Flow in the Sheeted dike Complex of Fast Spreading Crust: Pervasive Fluid Flow at Pito Deep. *Geochemistry Geophysics. Geosystems* 9, 1–19. doi: 10.1029/2007gc001901

Bekele, A., and Schmerold, R. (2020). Characterization of brines and evaporite deposits for their lithium contents in the northern part of the Danakil Depression and in some selected areas of the Main Ethiopian Rift Lakes. *J. Afr. Earth Sci.* 170, 103904. doi: 10.1016/j.jafrearsci.2020.103904

Bernath, P., Boone, C., Pastorek, A., Cameron, D., and Lecours, M. (2023). Satellite characterization of global stratospheric sulfate aerosols released by Tonga volcano. *J. Quantitative Spectrosc. Radiative Transfer* 299, 108520. doi: 10.1016/j.jqsrt.2023.108520

Bonnet, S., Caffin, M., Berthelot, H., and Moutin, T. (2017). Hot spot of N_2 fixation in the western tropical South Pacific pleads for a spatial decoupling between N_2 fixation and denitrification. *Proc. Natl. Acad. Sci.* 114, 14 E2800–E2801. doi: 10.1073/pnas.1619514114

Bonnet, S., Guieu, C., Taillandier, V., Boulart, C., Bouruet-Aubertot, P., Gazeau, F., et al. (2023). Natural iron fertilization by shallow hydrothermal sources fuels diazotroph blooms in the ocean. *Science* 380, 812–817. doi: 10.1126/science.abq4654

Brandl, P. A., Schmid, F., Augustin, N., Grevemeyer, I., Arculus, R. J., Devey, C. W., et al. (2020). The 6–8 aug 2019 eruption of 'Volcano F' in the tofua arc, Tonga. *J. Volcanology Geothermal Res.* 390, 106695. doi: 10.1016/j.jvolgeores.2019.106695

Brunskill, G. J., Zagorskis, I., and Pfitzner, J. (2003). Geochemical mass balance for lithium, boron, and strontium in the gulf of papua, papua new Guinea (Project TROPICS). *Geochimica Cosmochimica Acta* 67, 3365–3383. doi: 10.1016/S0016-7037(02)01410-2

Chan, L.-H., and Hein, J. R. (2007). Lithium contents and isotopic compositions of ferromanganese deposits from the global ocean. *Deep Sea Res. Part II: Topical Stud. Oceanography* 54, 1147–1162. doi: 10.1016/j.TSr2.2007.04.003

Chavagnac, V., Leleu, T., Fontaine, F., Cannat, M., Ceuleneer, G., and Castillo, A. (2018a). Spatial variations in vent chemistry at the lucky strike hydrothermal field, mid-atlantic ridge (37°N): updates for subseafloor flow geometry from the newly discovered capelinhos vent. *Geochemistry Geophysics Geosystems* 19, 4444–4458. doi: 10.1029/2018GC007765

Chen, D., Thibon, F., Felbacq, A., Weppe, L., Metian, M., and Vigier, N. (2023). Coupled survey of lithium isotopes and Li/Ca in biogenic and inorganic carbonates. *Earth Sci. Rev.* 244, 104500. doi: 10.1016/j.earscirev.2023.104500

Clare, M. A., Yeo1, I. A., Watson, S., Wysoczanski, R., Seabrook, S., Mackay, K., et al. (2023). Fast and destructive density currents created by ocean-entering volcanic eruptions. *Science* 381, 1085–1092. doi: 10.1126/science.adi3038

Colombier, M., Mueller, S. B., Kueppers, U., Scheu, B., Delmelle, P., Cimarelli, C., et al. (2019). Diversity of soluble salt concentrations on volcanic ash aggregates from a variety of eruption types and deposits. *Bull. Volcanology* 81, 39. doi: 10.1007/s00445-019-1302-0

Davis, A. C., Bickle, M. J., and Teagle, D. A. H. (2003). Imbalance in the oceanic strontium budget. *Earth Planetary Sci. Lett.* 211, 173–187. doi: 10.1016/S0012-821X(03)00191-2

Delmelle, P., Lambert, M., Dufrêne, Y., Gerin, P., and Óskarsson, N. (2007). Gas/aerosol–ash interaction in volcanic plumes: New insights from surface analyses of fine ash particles. *Earth Planetary Sci. Lett.* 259, 159–170. doi: 10.1016/j.epsl.2007.04.052

Delmelle, P., Wadsworth, F. B., Maters, E. C., and Ayris, P. M. (2018). High temperature reactions between gases and ash particles in volcanic eruption plumes. *Rev. Mineralogy Geochemistry* 84, 285–308. doi: 10.2138/rmg.2018.84.8

Dutay, J.-C., Jean-Baptiste, P., Campin, J.-M., Ishida, A., Maier-Reimer, E., Matear, R. J., et al. (2004). Evaluation of OCMIP-2 ocean models' deep circulation with mantle helium-3. *J. Mar. Syst.* 48, 15–36. doi: 10.1016/j.jmarsys.2003.05.010

El Meknassi, S., Dera, G., Cardone, T., De Rafélis, M., Brahmi, C., and Chavagnac, V. (2018). isotope ratios of modern carbonate shells: Good and bad news for chemostratigraphy. *Geology* 46, 1003–1006. doi: 10.1130/G45380.1

Escrig, S., Bézos, A., Langmuir, C. H., Michael, P. J., and Arculus, R. (2012). Characterizing the effect of mantle source, subduction input and melting in the Fonualei Spreading Center, Lau Basin: Constraints on the origin of the boninitic signature of the back-arc lavas. *Geochemistry Geophysics Geosystems* 13, 10. doi: 10.1029/2012GC004130

Falkenberg, J. J., Keith, M., Haase, K. M., Sporer, C., Bach, W., Klemd, R., et al. (2022). Spatial variations in magmatic volatile influx and fluid boiling in the submarine hydrothermal systems of niuatahi caldera, Tonga rear-arc. *Geochemistry Geophysics Geosystems* 23, e2021GC010259. doi: 10.1029/2021GC010259

Garcia, M. G., Borda, L. G., Godfrey, L. V., López Steinmetz, R. L., and Losada-Calderon, A. (2020). Characterization of lithium cycling in the Salar De Olaroz, Central Andes, using a geochemical and isotopic approach. *Chem. Geology* 531, 119340. doi: 10.1016/j.chemgeo.2019.119340

German, C. R., Casciotti, K. A., Dutay, J., Heimbürger, L. E., Jenkins, W. J., Measures, C. I., et al. (2016). Hydrothermal impacts on trace element and isotope ocean biogeochemistry. *Philos. Trans. R. Soc. A.* 374, 20160035. doi: 10.1098/rsta.2016.0035

Global Volcanism Program (2019). "Report on lateiki (Tonga)," in *Weekly volcanic activity report, 9 october-15 october 2019*. Ed. S. K. Sennert (Washington DC: Smithsonian Institution and US Geological Surve). Available at: https://volcano.si.edu/showreport.cfm?wvar=GVP.WVAR20191009-243070.

Guieu, C., and Bonnet, S. (2019). TONGA 2019 cruise report, L'Atalante R/V. *SEANOE*. 74. doi: 10.17600/18000884

Guieu, C., Bonnet, S., Petrenko, A., Menkes, C., Chavagnac, V., Desboeufs, K., et al. (2018). Iron from a submarine source impacts the productive layer of the Western Tropical South Pacific (WTSP). *Sci. Rep.* 8, 9075. doi: 10.1038/s41598-018-27407-z

Guieu, C., Bonnet, S., Abadou, F., Alliouane, S., Arnaud-Haond, S., Arnone, V., et al. (2023). *Biogeochemical dataset collected during the TONGA cruise* (SEANOE). doi: 10.17882/88169

Huh, Y., Chan, L.-H., Zhang, L., and Edmond, J. M. (1998). Lithium and its isotopes in major world rivers: implications for weathering and the oceanic budget. *Geochimica Cosmochimica Acta* 62, 2039–2051. doi: 10.1016/S0016-7037(98)00126-4

Humphris, S. E., and Bach, W. (2005). On the Sr isotope and REE compositions of anhydrites from the TAG seafloor hydrothermal system. *Geochimica Cosmochimica Acta* 69, 1511–1525. doi: 10.1016/j.gca.2004.10.004

James, R. H., and Palmer, M. R. (2000). The lithium isotope composition of international rock standards. *Chem. Geology* 166, 319–326. doi: 10.1016/S0009-2541(99)00217-X

Leleu, T. (2017). *Variabilitè spatio-temporelle de la composition des fluides hydrothermaux (observatoire fond de mer EMSO-Açores, Lucky Strike): Traçage de la circulation hydrothermale et quantification des flux chimiques associés. Ph.D. Thesis, University of Toulouse III Paul Sabatier*. (Toulouse: University of Toulouse III Paul Sabatier).

Lowenstern, J. B., Bleick, H., Vazquez, J. A., Castro, J. M., and Larson, P. B. (2012). Degassing of Cl, F, Li, and Be during extrusion and crystallization of the rhyolite dome at Volcán Chaitén, Chile during 2008 and 2009. *Bull. Volcanology* 74, 2303–2319. doi: 10.1007/s00445-012-0663-4

Lupton, J., Lilley, M., Butterfield, D., Evans, L., Embley, R., Massoth, G., et al. (2008). Venting of a separate CO_2 -rich gas phase from submarine arc volcanoes: Examples from the Mariana and Tonga-Kermadec arcs. *J. Geophysical Res.* 113, B8. doi: 10.1029/2007JB005467

Massoth, G., Baker, E., Worthington, T., Lupton, J., De Ronde, C., Arculus, R., et al. (2007). Multiple hydrothermal sources along the south Tonga arc and Valu Fa Ridge. . *Geochemistry Geophysics Geosystems* 8, 11. doi: 10.1029/2007GC001675

Millot, R., Petelet-Giraud, E., Guerrot, C., and Négrel, P. (2010a). Multi-isotopic composition (δ^7Li–δ^{11}B–δD–δ^{18}O) of rainwaters in France: Origin and spatio-temporal characterization. *Appl. Geochemistry* 25, 1510–1524. doi: 10.1016/j.apgeochem.2010.08.002

Millot, R., Scaillet, B., and Sanjuan, B. (2010b). Lithium isotopes in island arc geothermal systems: Guadeloupe, Martinique (French West Indies) and experimental approach. *Geochimica Cosmochimica Acta* 74, 1852–1871. doi: 10.1016/j.gca.2009.12.007

Misra, S., and Froelich, P. N. (2012). Lithium isotope history of Cenozoic seawater: changes in silicate weathering and reverse weathering. *Science* 335, 818–823. doi: 10.1126/science.1214697

Newland, E. L., Mingotti, N., and Woods, A. W. (2022). Dynamics of deep-submarine volcanic eruptions. *Sci. Rep.* 12, 3276. doi: 10.1038/s41598-022-07351-9

Nonell, A., Toutain, J.-P., Polvé, M., Munoz, M., and Berger, G. (2005). First coupled Sr and Pb isotopic measurements in volcanic gas condensates and groundwaters of Vulcano Island (Italy). *Geochemistry Geophysics Geosystems* 6, 11. doi: 10.1029/2005GC000980

Oppenheimer, C. (2003). "Volcanic degassing," in *The crust. Treatise in geochemistry*, vol. 3 . Ed. R. L. Rudnick (Elsevier), 123–166.

Palmer, M. R., and Edmond, J. M. (1989). The strontium isotope budget of the modern ocean. *Earth Planetary Sci. Lett.* 92, 11–26. doi: 10.1016/0012-821X(89)90017-4

Pin, C., Gannoun, A., and Dupont, A. (2014). Rapid, simultaneous separation of Sr, Pb, and Nd by extraction chromatography prior to isotope ratios determination by TIMS and MC-ICP-MS. *J. Analytical Atomic Spectrometry* 29, 1858–1870. doi: 10.1039/C4JA00169A

Plank, S., Marchese, F., Genzano, N., Nolde, M., and Martinis, S. (2020). The short life of the volcanic island New Late'iki (Tonga) analyzed by multi-sensor remote sensing data. *Sci. Rep.* 10, 22293. doi: 10.1038/s41598-020-79261-7

Poet, M., Vigier, N., Bouret, Y., Jarretou, G., Gautier, R., Bendahhou, S., et al. (2023). Biological fractionation of lithium isotopes by cellular Na^+/H^+ exchangers unravels fundamental transport mechanisms. *iScience* 26, 106887. doi: 10.1016/j.isci.2023.106887

Rose, W. I. (1977). Scavenging of volcanic aerosol by ash: atmospheric and volcanologic implications. *Geology* 5, 621–624. doi: 10.1130/0091-7613(1977)5<621:SOVABA>2.0.CO;2

Rosner, M., Ball, L., Peucker-Ehrenbrink, B., Blusztajn, J., Bach, W., and Erzinger, J. (2007). A simplified, accurate and fast method for lithium isotope analysis of rocks and fluids, and δ^7Li values of seawater and rock reference materials. *Geostandards Geoanalytical Res.* 31, 77–88. doi: 10.1111/j.1751-908X.2007.00843.x

Ryan, W. B. F., Carbotte, S. M., Coplan, J. O., O'Hara, S., Melkonian, A., Arko, R., et al. (2009). Global multi-resolution topography synthesis. *Geochemistry Geophysics Geosystems* 10, 3. doi: 10.1029/2008GC002332

Stewart, C., Damby, D. E., Horwell, C. J., Elias, T., Ilyinskaya, E., Tomašek, I., et al. (2022). Volcanic air pollution and human health: recent advances and future directions. *Bull. Volcanology* 84, 11. doi: 10.1007/s00445-021-01513-9

Stewart, C., Damby, D. E., Tomašek, I., Horwell, C. J., Plumlee, G. S., Armienta, M. A., et al. (2020). Assessment of leachable elements in volcanic ashfall: a review and evaluation of a standardized protocol for ash hazard characterization. *J. Volcanology Geothermal Res.* 392, 106756. doi: 10.1016/j.jvolgeores.2019.106756

Stoffers, P., Worthington, T. J., Schwarz-Schampera, U., Hannington, M. D., Massoth, G. J., Hekinian, R., et al. (2006). Submarine volcanoes and high-temperature hydrothermal venting on the Tonga arc, southwest Pacific. *Geology* 34, 453. doi: 10.1130/G22227.1

Stoffers, P., Worthington, T., Shipboard Scientific Party (2003). "Cruise report SONNE 167, louisville," in *Louisville Ridge: Dynamics and magmatism of a mantle plume and its influence on the Tonga-Kermadec Subduction System* (Kiel Christian-Albrechts-Universität, Suva, Fiji – Wellington, New Zealand), 276, ISBN: .

Symonds, R. B., Rose, W. I., Bluth, G. J., and Gerlach, T. M. (1994). Volcanic-gas studies: Methods, results, and applications. *Mineralogical Soc. America* 30, 1–66.

Symonds, R. B., Rose, W. I., and Reed, M. H. (1988). Contribution of C1- and F-bearing gases to the atmosphere by volcanoes. *Nature* 334, 415–418. doi: 10.1038/334415a0

Taillandier, V., Wagener, T., D'Ortenzio, F., Mayot, N., Legoff, H., Ras, J., et al. (2018). Hydrography and biogeochemistry dedicated to the Mediterranean BGC-Argo network during a cruise with RV Tethys 2 in May 2015. *Earth System Sci. Data* 10, 627–641. doi: 10.5194/essd-10-627-2018

Thibon, F., Metian, M., Oberhänsli, F., Montanes, M., Vassileva, E., Orani, A. M., et al. (2021). Bioaccumulation of lithium isotopes in mussel soft tissues and implications for coastal environments. *ACS Earth Space Chem.* 5, 1407–1417. doi: 10.1021/acsearthspacechem.1c00045

Tilliette, C., Gazeau, F., Chavagnac, V., Leblond, N., Montanes, M., Leblanc, K., et al. (2023a). Temporal and spatial variability in the hydrothermal signature of sinking particles and sediments in the Western Tropical South Pacific Ocean. *J. Geophysical Res. – Oceans* 128, e2023JC019828. doi: 10.1029/2023JC019828

Tilliette, C., Gazeau, F., Portlock, G., Benavides, M., Bonnet, S., Guigue, C., et al. (2023b). Influence of shallow hydrothermal fluid release on the functioning of phytoplankton communities. *Front. Mar. Sci.* 10. doi: 10.3389/fmars.2023.1082077

Tilliette, C., Taillandier, V., Bouruet-Aubertot, P., Grima, N., Maes, C., Montanes, M., et al. (2022). Dissolved iron patterns impacted by shallow hydrothermal sources along a transect through the Tonga-kermadec arc. *Global Biogeochemical Cycles* 36, e2022GB007363. doi: 10.1029/2022GB007363

Tomascak, P. B., Magna, T., and Dohmen, R. (2016). *Advances in lithium isotope geochemistry, advances in isotope geochemistry* (Springer International Publishing). doi: 10.1007/978-3-319-01430-2

Vance, D., Teagle, D. A. H., and Foster, G. L. (2009). Variable Quaternary chemical weathering fluxes and imbalances in marine geochemical budgets. *Nature* 458, 493–496. doi: 10.1038/nature07828

Vigier, N., Decarreau, A., Millot, R., Carignan, J., Petit, S., and France-Lanord, C. (2008). Quantifying li isotope fractionation during smectite formation and implications for the li cycle. *Geochimica Cosmochimica Acta* 72, 780–792. doi: 10.1016/j.gca.2007.11.011

Vigier, N., Rollion-Bard, C., Levenson, Y., and Erez, J. (2015). Lithium isotopes in foraminifera shells as novel proxy for the ocean dissolved inorganic carbon (DIC). *Comptes Rendu Geosci.* 347, 43–51. doi: 10.1016/j.crte.2014.12.001

Vigier, N., Weppe, L., Tilliette, C., Chavagnac, V., Boulart, C., Thibon, F., et al. (2022). "Impact of shallow hydrothermalism on lithium content and lithium isotope composition of marine plankton," in *Goldschmidt Conference*. doi: 10.46427/gold2022.11142

Wakaki, S., Obata, H., Tazoe, H., and Ishikawa, T. (2017). Precise and accurate analysis of deep and surface seawater Sr stable isotopic composition by double-spike thermal ionization mass spectrometry. *Geochemical J.* 51, 227–239. doi: 10.2343/geochemj.2.0461

Wilckens, F. K., Reeves, E. P., Bach, W., Seewald, J. S., and Kasemann, S. A. (2019). Application of B, mg, li and sr isotopes in acid-sulfate vent fluids and volcanic rocks as tracers for fluid-rock interaction in back-arc hydrothermal systems. *Geochemistry Geophysics Geosystems* 20, 5849–5866. doi: 10.1029/2019GC008694

Zhu, Y., Toon, O. B., Jensen, E. J., Bardeen, C. G., Mills, M. J., Tolbert, M. A., et al. (2020). Persisting volcanic ash particles impact stratospheric SO_2 lifetime and aerosol optical properties. *Nat. Communication* 11, 4526. doi: 10.1038/s41467-020-18352-5